Chaos in reversed-field-pinch plasma simulation and experiment

Christopher Watts,* D. E. Newman,† and J. C. Sprott

Department of Physics, University of Wisconsin—Madison, Madison, Wisconsin 53706

(Received 4 October 1993)

We investigate the possibility that chaos and simple determinism are governing the dynamics of reversed-field-pinch (RFP) plasmas using data from both numerical simulations and experiment. A large repertoire of nonlinear-analysis techniques is used to identify low-dimensional chaos. These tools include phase portraits and Poincaré sections, correlation dimension, the spectrum of Lyapunov exponents, and short-term predictability. In addition, nonlinear-noise-reduction techniques are applied to the experimental data in an attempt to extract any underlying deterministic dynamics. Two model systems are used to simulate the plasma dynamics. These are the DEBS computer code, which models global RFP dynamics, and the dissipative trapped-electron-mode model, which models drift-wave turbulence. Data from both simulations show strong indications of low-dimensional chaos and simple determinism. Experimental data were obtained from the Madison Symmetric Torus RFP and consist of a wide array of both global and local diagnostic signals. None of the signals shows any indication of low-dimensional chaos or other simple determinism. Moreover, most of the analysis tools indicate that the experimental system is very high dimensional with properties similar to noise. Nonlinear noise reduction is unsuccessful at extracting an underlying deterministic system.

PACS number(s): 52.55.Ez, 52.65.+z, 47.52.+j, 05.45.+b

I. INTRODUCTION

The search for evidence of chaos in plasmas has yielded mixed results. A wide range of chaotic processes has been reported, including the transition to turbulence and the formation of magnetic islands [1]. Several groups have reported chaos and period-doubling behavior in glow discharges and pulsed machines [2–5]. Low-dimensional chaos has also been identified with drift-wave turbulence both in experiment [6] and simulations [7]. In toroidal, fusion-relevant devices chaos has been reported in low-frequency magnetic-field oscillations in the DITE tokamak [8] and in broadband (0–100 kHz) magnetic-field oscillations in the HBTX1A reversed-field pinch (RFP) [9]. In the TFTR device low-dimensional chaos has been reported in density fluctuations, with the dimension dependent on the wave number [10]. In contrast, broadband magnetic and density fluctuations in the TCA tokamak show no evidence of low-dimensional chaos [11].

In this paper we examine the possibility that chaos or other simple determinism governs the dynamics of RFP discharges using data from both experiment and numerical simulations. Simulations suggest that chaos should be present in RFP discharges. However, it eludes all tests for identification in experimental data. As will be dis-

cussed, identification is particularly sensitive to the presence of noise and the stationarity of the system. This is additionally complicated by the fact that standard linear filtering techniques are not appropriate to signals generated by chaotic systems. Thus, although low-dimensional chaos may govern Madison Symmetric Torus (MST) discharges, it cannot be identified by the analysis techniques.

The MST [12] reversed-field pinch provides a particularly good instrument for investigations in nonlinear dynamics in fusion plasmas. It is a large toroidal confinement device with discharges characterized by a spontaneous reversal of the toroidal magnetic field at the edge of the plasma. Although most measured quantities are characterized by broadband frequency spectra, most of the fluctuation power (ca. 90%) is concentrated in a few long-wavelength spatial modes. Experimental evidence and numerical simulations suggest that the mechanism behind these tearing mode fluctuations is a three-wave coupling process, linking two $m = 1$ modes to an $m = 2$ mode [13]. This corroboration of experiment and code indicates that the dominant plasma processes can be modeled as a deterministic system.

The past decade has seen a tremendous effort towards correlating experimentally observed transport with computational models. Drift-wave models in particular have shown promise towards explaining the anomalous ion heat loss in tokamaks. Previous studies of these models indicate that the dynamics are low dimensional, despite the large number of interacting modes in the system [7]. The applicability of drift-wave models to RFP transport is more tenuous. However, the models have sufficiently general nonlinear dynamics that many of the results should be relevant to RFP physics.

The paper is organized as follows: Section II reviews

_____

*Present address: Fusion Research Center, Robert L. Moore Bldg., University of Texas, Austin, TX 78712. Electronic address: watts@fusion.ph.utexas.edu

†Present address: Fusion Energy Division, M.S. 8071, P.O. Box 2009, Oak Ridge National Laboratory, Oak Ridge, TN 37831-8076.

the techniques to be used in our analysis of the data. Section III presents the results from analysis of two numerical simulations. The DEBS computer code simulates RFP plasmas and is thought to model correctly the dominant tearing mode fluctuations. The dissipative trapped-electron-mode (DTEM) model is designed to model drift-wave turbulence thought to be a major contributor to transport in the core of tokamaks. Section IV presents the results of analysis of experimental data from the MST. In the final section we discuss the results.

II. ANALYSIS METHODS

To ascertain whether or not low-dimensional chaos governs RFP discharges, several analysis techniques are used. These include calculation of the correlation dimension and the spectrum of Lyapunov exponents and assessing the short-term predictability. Analysis is also performed on surrogate data records to guard against spurious determinations of low-dimensional chaos. In addition, nonlinear-noise-reduction techniques are applied to the experimental data in an attempt to detect a low-dimensional system in noise corrupted data. The methods used will be outlined in this section.

In general, one does not have access to all the independent variables of the system, and for experimental data, it may not be clear *which* variables are independent. Takens has proven that for dynamical systems, a single variable will capture all the relevant dynamics of the system subject to certain conditions [14]. Specifically, given a system whose trajectory $F(t)=(x(t),y(t),z(t),...)$ lies on an attractor there is a differentiable, reversible mapping from the manifold containing the attractor to that containing the attractor in delayed coordinates $X(t)=(x(t),x(t+\tau),x(t+2\tau),...,x(t+m\tau))$, so long as $m \geq 2d+1$, where d is the dimension containing the original attractor and m is the dimension of the embedding space. The necessity of $2d+1$ components is to ensure that the vectors span the embedding space. Values of m less than $2d+1$ often suffice for proper reconstruction of the system.

Critical in implementing all analysis procedures outlined in this section is the proper choice of the time lag τ. For a finite data record, the time lag must be chosen such that vector components are independent. Choosing τ too small can result in artificially high correlation, and conversely, because chaotic systems are characterized by sensitivity to initial conditions, too large a value of τ leads to extreme decorrelation. A good criterion is τ times the embedding dimension should be 2 to 3 times the exponential-folding time of the autocorrelation function. However, all analysis procedures are performed using several values of τ to find an optimal value. Typically, there is a range of window lengths $(m-1)\tau$ over which the quantity being measured can be accurately estimated. There is an excellent discussion in Albano, Muench, and Schwartz [15] as this applies to the correlation dimension.

Furthermore, the data should be sampled frequently enough so that the autocorrelation time is several time steps. Infrequent sampling will yield data that are im-

properly correlated; sampling too often will confine the dynamics to only a portion of the attractor. Best results for all analysis methods presented here are obtained when the autocorrelation time is around 10 to 20 time steps.

A. Correlation dimension

We estimate the fractal dimension of the data using the correlation dimension of Grassberger and Proccacia [16]. It is defined by

$$D_2 = \lim_{r \to 0} \frac{\log_{10} C(r)}{\log_{10} r} , \tag{1}$$

where

$$C(r) = \lim_{N \to \infty} \frac{1}{N^2} \sum_{i \neq j} \Theta(r - |x_i - x_j|) , \tag{2}$$

and $\Theta(r)$ is the Heavyside function whose value is one for $r > 0$, and zero otherwise, and N is the number of points. The correlation dimension provides a lower bound on the Hausdorff (fractal) dimension. The two often agree closely, differing by no more than a few percent.

Typically, one computes the correlation integral for various radii r and plots $\log_{10} C(r)$ vs $\log_{10} r$. Over some region in $\log_{10} r$, known as the scaling region, the slope is constant, and the value of this slope is taken as the correlation dimension. The two-point slope $d[\log_{10} C(r)]/d[\log_{10} r]$ vs $\log_{10} r$ is more often informative. This yields a plateau at the value of the correlation dimension, allowing a better determination of the scaling region.

Several groups have estimated the number of points required for a reliable determination of the correlation dimension. Estimates range from several hundred [17] to 42^d [18]. Tsonis provides a more reasonable rule: $N_{min} \propto 10^{2+0.4d}$ [19]. We use a criterion based on the length of the scaling region. For adequate confidence in a correlation-dimension determination a scaling region should span at least a decade in r [20].

B. Lyapunov exponents

The Lyapunov exponents measure the average divergence and convergence of orbits in phase space. Nearby trajectories of chaotic systems will, on average, diverge or converge exponentially in time. For the one-dimensional continuous map $x(t)=f_t(x_0)$, with two initial conditions separated by δx the average separation after a time t is $\delta x_t \approx \delta x_0 e^{\lambda t}$. Taking the limit of infinitesimally separated points and infinite time the characteristic or Lyapunov exponent λ is defined by

$$\lambda = \lim_{t \to \infty} \frac{1}{t} \lim_{\delta x_0 \to 0} \ln \left| \frac{\delta x_t}{\delta x_0} \right| = \lim_{t \to \infty} \frac{1}{t} \ln \left| \frac{df_t(x)}{dx} \right| . \tag{3}$$

A positive largest Lyapunov exponent has become the standard definition of a chaotic system.

For systems of more than one dimension there is a spectrum of Lyapunov exponents where each exponent corresponds to one of the principal axes of an ellipsoid centered on the trajectory and characterizes the local ex-

pansion or contraction of the attractor. The orientation of this ellipsoid changes as the trajectory evolves in time. The spectrum of Lyapunov exponents is given by

$$\lambda^{(k)} = \lim_{t \to \infty} \frac{1}{t} \ln \left| \frac{\partial f_t(x^{(k)})}{\partial x^{(k)}} \right| = \lim_{t \to \infty} \frac{1}{t} \ln \|J_t^{(k)}\|$$

$$k = 1, 2, \ldots, d , \qquad (4)$$

where $\|J_t^{(k)}\|$ is the kth eigenvalue of the d-dimensional Jacobian after advancing the system a time t (see [21] for a thorough discussion).

Any continuous chaotic system must have at least three dimensions and hence three Lyapunov exponents. If the system is dissipative their sum must be negative to reflect the contraction of phase space. The least negative exponent controls the rate at which perturbed trajectories approach the inertial manifold [22]. A chaotic system has a positive largest exponent, and any system continuous in time must have at least one Lyapunov exponent equal to zero corresponding to the lack of divergence (on average) tangent to the flow [23]. Thus a three-dimensional chaotic system has Lyapunov exponents $(+, 0, -)$.

Wolf et al. [22] have developed a method for a calculating the largest exponent from the time series of a single variable of the chaotic system. The method follows a fiducial trajectory of the system and calculates the average separation of neighboring trajectories as they evolve. Although the procedure is effective, it is incomplete. A single Lyapunov exponent can only indicate that a system is chaotic, but tells nothing about the dimension of the system. Noise also has a positive largest Lyapunov exponent. One needs the entire spectrum of exponents to ascertain whether or not simple determinism exits.

A method proposed by Eckmann et al. [24] and modified by Briggs [25] computes the spectrum of exponents by approximating the Jacobian of the local trajectory of the dynamical system. In the method of Briggs, the time series is embedded in delay space, a group of nearest neighbors is found, and their trajectory is fit to a polynomial. This function can then be differentiated analytically to obtain the Jacobian of the local dynamics.

Finding the eigenvalues of real, nonsymmetric matrices is not trivial, and often the eigenvalues are complex, whereas Lyapunov exponents are real. This is because the tangent space of the system is not necessarily aligned with our (arbitrary) coordinate system. Computation of the Lyapunov exponents is facilitated by QR decomposition. Any matrix can be written as $\mathbf{M} = \mathbf{QR}$, where $\mathbf{Q}$ is an orthogonal matrix and $\mathbf{R}$ is upper right triangular with positive diagonal elements. This is known as the "skinny" decomposition, and it is unique. Since the time series to be analyzed is discretized, the Jacobian, using the chain rule, can be written as $\mathbf{J}_{t+1} = [\partial f_{t+1}/\partial x] = \mathbf{J}_t \mathbf{J}_{t-1} \cdots \mathbf{J}_1 = \mathbf{Q}_{(t)} \mathbf{R}_{(t)} \cdots \mathbf{R}_{(2)} \mathbf{R}_{(1)}$. The effect of the products $\mathbf{JQ}$ is to successively orient the Jacobian matrices along the principal axes of the tangent space of the attractor. The Lyapunov exponents are then given by

$$\lambda_i = \frac{1}{\tau n} \sum_{j=1}^{n} \ln R_{ii(j)} . \qquad (5)$$

Implementation of the algorithm is not difficult on a computer, and several routines exist to do the QR decomposition [26,27]. Most of the CPU time is spent searching for nearest neighbors rather than in actual calculation of the exponent. The Briggs method gives superior results to the original method proposed by Eckmann and Ruelle, because in fitting an arbitrary polynomial it includes the curvature of the local space. This is particularly relevant in embedding dimensions higher than the spatial dimension of the attractor.

Kaplan and Yorke [28] have conjectured a general formula that relates the Lyapunov exponents to the fractal dimension, D_0,

$$D_{KY} = j + \frac{\sum_{i=1}^{j} \lambda_i}{|\lambda_{j+1}|} \approx D_0 , \qquad (6)$$

where D_{KY} is the Kaplan-Yorke or Lyapunov dimension. The Lyapunov exponents are ordered such that $\lambda_i > \lambda_{i+1}$, and j is the largest index for which $\sum_{i=1}^{j} \lambda_i > 0$. The conjecture appears to hold rigorously only for homogeneous attractors. However, it does hold approximately for many cases.

In calculating the spectrum of exponents, there are several indications that the system is deterministic and not random. First, in higher embedding spaces the values of the exponents will remain reasonably constant, and additional exponents will be negative. A direct consequence of this is that the Kaplan-Yorke dimension statures to a nearly constant value. In addition, continuous systems will have an exponent close to zero. Randomness can be identified by several characteristics. The data fill the space they are embedded in, as evidenced by the KY dimension, and although there are negative exponents, no convincing zero exponent exists. Negative exponents reflect the fact that the system is bounded. Moreover, it is difficult to find sufficient nearest neighbors, even for rather large radii because random points are sparsely and evenly distributed in the embedding space.

C. Nonlinear prediction

One goal of identifying and characterizing chaotic behavior in experimental data is to develop a set of model equations for the system. A less ambitious goal is simply to predict the short-term behavior without knowing the governing equations explicitly. With this goal in mind, several methods have been developed, all of which use essentially the same procedure, with more or less sophistication [29–31]. The time series is first embedded in an appropriate space using the method of time lags. The initial point for prediction is chosen, and the space is searched for its nearest neighbors. In the simplest method, the average of the neighbor's short-term trajectory becomes the basis for predicting the evolution of the initial point. The neighbors of this new point are then found, and the process is repeated. A superior method fits a linear or higher-order polynomial to the local trajec-

tory. We use a method similar to one proposed by Farmer and Sidorowich [29] except that a generalized polynomial is fit to the local trajectory. The generalized polynomial can be written as

$$F_i(x) = f_{i0} + \sum f_{i1}x + \sum f_{i2}xx + \cdots , \tag{7}$$

where $F_i(x)$ is the map of the ith component and the sums are over all components in the embedding space (f_{i1} is an m dimensional vector, f_{i2} is an $m \times m$ tensor, etc.).

To measure the predictability we compute the average deviation of the predicted from the actual values, normalized to the distance propagated:

$$e_{\text{predict}} = \frac{|y - x|}{|x|} , \tag{8}$$

where y is a vector pointing along the predicted orbit and x points along the actual orbit. Because a single poor prediction (say, in a sparsely populated region of phase space) can strongly skew the mean, the median is a better measure of the average normalized deviation. Predictions are done at successive time steps measured in units of $\tau - 1$ for two reasons. Colored-noise systems, particularly low-pass filtered noise, can give very small prediction errors if the time step is too small. Choosing the time step equal to τ, however, will result in spurious correlations because components are shared among successive vectors. Hence the choice of $\tau - 1$. Despite this choice, correlated noise (random systems with short-term correlation, e.g., colored noise) will show some short-term predictability. White noise consistently has 100% error.

D. Surrogate data sets

Once a chaotic system has been identified, one needs to confirm that the identification is not an artifact of the analysis procedure. One method for doing so involves the creation of surrogate data sets. A surrogate set is similar to the original data, but randomized in some way to destroy the determinism. The analysis methods should then be reapplied to this new data set. All tests should yield negative results, thereby confirming the original assessment of determinism. If there still reman indications of determinism, one is likely witnessing an artifact of the analysis method.

The most effective method of creating a surrogate involves using the data from the original system and randomizing the phases of the Fourier components. This preserves the original power spectrum, but creates a data set in which small-scale spatial structure is lost. The methods preserves global quantities of the system: the power spectrum (obviously), macrostructure in all embeddings (similar periodicity and amplitude), and also the autocorrelation time. Yet any simple determinism is destroyed.

E. Nonlinear noise reduction

While simple low-pass filtering may be appropriate in most cases, in general it is an inferior method of noise reduction. This is because it does not take into account

the inherent nonlinear dynamics of the system. The method simply attenuates all signal components greater than a certain frequency. This may, however, alter the relevant dynamics of the system while ignoring other spurious components at lower frequencies. In addition, linear filtering methods can distort the phase information. As discussed in the previous section, this information is crucial to the dynamics of chaotic trajectories.

Several similar alternative methods of filtering specifically aimed at reducing noise in chaotic systems have been developed [32–38]. The methods make use of the spatial structure of the underlying attractor and are similar in implementation to the prediction methods outlined in Sec. II C. The time record of a single variable of the system is embedded using the method of lags. For each point in the embedding space the nearest neighbors are found. The average local trajectory of these points is found, which becomes the functional map of the point being filtered.

The method as outlined lacks self-consistency, however. One begins with a single time record and creates from it an array of time records, one corresponding to each dimension of the embedding space. The method for correcting this distinguishes the various approaches. One approach simply updates only a few of the components in the embedded space. For a given point in the embedded space $(x(t), x(t+\tau), x(t+2\tau), \ldots)$, the filtered image point is $(y(t+\Delta t), y(t+\Delta t+\tau), \ldots, x(t+\Delta t + n\tau), \ldots)$, where y is the filtered signal. Thus, each new basis vector consists of some components from the filtered trajectory and the remaining components from the original signal. Our investigations indicate that updating only one, the leading component, yields the best results. The method is iterative, with several iterations required for best results. It achieves very good results for sets of ordinary differential equations with modest levels of additive noise ($< 100\%$), recovering the original trajectory very nearly. The global deterministic properties of the system—fractal dimension, Lyapunov spectrum, and short-term predictability—are only partially recovered, since some small scale structure is lost. However, it is sufficient to be able to recognize the system as low dimensional.

More sophisticated methods to achieve self-consistency use a window of points and find the best fit trajectory using a least-squares method [32,37]. Our investigations indicate that results are not much better than the above method.

III. NUMERICAL SIMULATIONS OF PLASMAS

In this section we present results from two numerical plasma simulations. The first is a code that models global RFP dynamics. The second is a model of drift-wave turbulence. Both systems show strong evidence of low-dimensional chaos.

A. DEBS code

The DEBS code is a three-dimensional magnetohydrodynamic (MHD) numerical simulation that with proper initialization will model reversed-field pinch discharges

[39–42]. The model has helped considerably in under-
standing tearing mode fluctuations in RFP plasmas. The
agreement between experiment and simulation lends
credibility to the code's ability to model real plasma pro-
cesses.

Although the code correctly models these phenomena,
there are some limitations. The model is pressureless,
and thus does not include pressure-driven modes. In ad-
dition, to have a reasonable computation time, the model
uses a rather small value for the magnetic Reynolds num-
ber, or Lundquist number $S = \tau_r/\tau_A$. τ_r is the resistive
diffusion time, given by $\tau_r = 4\pi a^2/c^2\eta$, where a is the
scale size of the system and η is the plasma resistivity.
τ_A is the Alfvén time and is equal to a divided by the
Alfvén speed $v_A = B_0/\sqrt{4\pi\rho_0}$, where ρ_0 is the density.
Larger values of S increase the computation time
significantly because the system becomes more turbulent
and requires a smaller time-step size to accurately follow
the wave dynamics. In the simulation presented here, the
Lundquist number was 6×10^3, whereas the experiment is
estimated to be the order of 10^6. Despite this low value,
several tens of Cray CPU hours are required for each run
to obtain a time record of sufficient length.

The code solves a reduced set of MHD equations via
the semi-implicit method. This method allows relatively
long time steps to track the relevant nonlinear phenome-
na by modifying the evolution of the destabilizing fast
time-scale Alfvén modes. Details of the method can be
found in the references. The dimensionless equations
solved are

$$\frac{\partial A}{\partial t} = SV \times B - \eta J \ ,$$

$$\rho\frac{\partial V}{\partial t} = -S\rho V \cdot \nabla V + SJ \times B + \nu\nabla^2 V \ .$$

(9)

The magnetic field B is in units of the characteristic field
strength B_0, V is the fluid velocity in units of the Alfvén
speed, A is the vector potential, J is the current density,
and ρ is the mass density in units of ρ_0. Finally, ν is the
viscosity coefficient $\nu = \nu_0\tau_r/a^2$, where ν_0 is the charac-
teristic viscosity. Both the viscosity and the mass density
are assumed to be spatially constant; furthermore, the
mass density is not evolved. The equations are solved in
cylindrical geometry with periodic boundary conditions
in the z direction to mimic a torus.

For the data presented here the equations were solved
for nine toroidal and three poloidal modes with 127 radi-
al mesh points. The system was monitored at regular in-
tervals during which nine quantities were recorded.
These were the parallel electric field $E_\parallel$, the average elec-
tric field $E_{ave} = -S\langle V \times B \rangle$, and the Ohmic electric field
$E_R = \eta J$ at both the edge and the core, the average
toroidal and poloidal magnetic fluctuations, dB_t/dt and
dB_p/dt, and toroidal loop voltage V_{loop}. We obtained
about 20 000 data points for each signal covering about
1.65 resistive diffusion times. Direct comparison with
MST discharges is not possible because of the compressed
time scales used in the code. However, by comparing
tearing mode time scales one arrives at a duration corre-
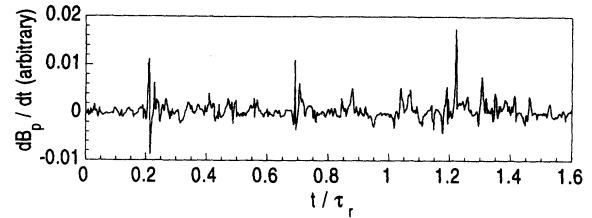sponding to about 55 ms for a standard MST discharge.

FIG. 1. Fluctuations of the poloidal magnetic field at the
wall from the DEBS code.

Figure 1 shows the time history of the average poloidal
magnetic field fluctuations. Time is measured in units of
the resistive diffusion time τ_r. The trace shows evidence
of flux jumps—bursts of magnetic field energy—which
are also characteristic of MST discharges. The power
spectrum of the signal is broadband, indicating that the
system is not periodic.

The correlation dimensions for dB_p/dt and its phase-
randomized surrogate are shown in Fig. 2. The original
signal shows a long plateau region with a value indepen-
dent of embedding dimension. The surrogate shows a
short region of spuriously low dimension, which is similar
to the behavior seen in correlated noise. Most other sig-
nals, including $E_\parallel$ and E_R, also have long plateaus of at
least a decade at a dimension between three and four.

The prediction errors for dB_p/dt, E_R, and their surro-
gates are plotted in Fig. 3. Both signals show fair predic-
tability, better by a factor of 3 than their corresponding
phase-randomized surrogates. However, an embedding
greater than 18 is required before any evidence of short-
term predictability is seen. This behavior is odd consid-
ering that the dimension of the system is no greater than
5, requiring an embedding of at most 11 to reconstruct
the attractor faithfully. This may be attributable to the
small number of data points.

Table I shows the Lyapunov exponents calculated for
two of the representative quantities. In both cases, the
Kaplan-Yorke dimension asymptotically approaches a
constant value, and the Lyapunov exponents remain rela-
tively constant as the embedding dimension increases.
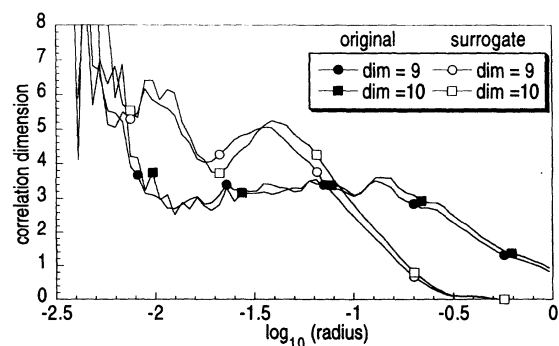Both systems show a clear zero exponent.

FIG. 2. Correlation dimension for dB_p/dt from the DEBS
code and its phase-randomized surrogate. The data show a scal-
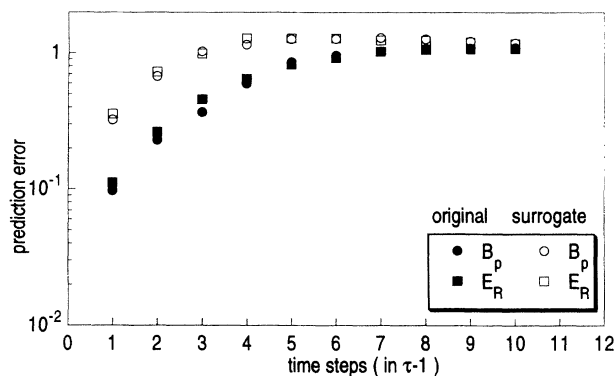ing region not present in the surrogate.

FIG. 3. Prediction error for the DEBS simulation. Predictability for both dB_p/dt and E_R is better by a factor of 3 than their surrogates.

B. Dissipative trapped-electron-mode (DTEM) model

A topic of intense research in the fusion plasma community is anomalous particle and energy transport. In tokamaks, one mechanism possibly responsible for this transport is the long-wavelength drift-wave turbulence associated with dissipative trapped ion and electron modes. The existence of these modes is indicated by several experiments [43–45], although their link to confinement is still speculative. The specific model is probably not directly applicable to RFP physics. However, the basic structure of the model provides an instructive archetype for long-wavelength turbulence in general. In particular, one of the nonlinearities, the polarization drift nonlinearity, has a direct correspondence to one of the MHD nonlinearities. Thus, although the model [46,47] differs in the details, some of the global properties—saturation, spectral distribution of energy, and transport—should be similar to those seen in RFP devices.

The DTEM model [46,47] possesses two nonlinearities that govern its behavior. These are the $E \times B$ nonlinearity and the polarization-drift nonlinearity. A similar model used to study η_i turbulence has been investigated for low-dimensional chaos in [7]. The DTEM model

equation is given by

$$\frac{\partial \tilde{n}}{\partial t} + v^* \frac{\partial \tilde{n}}{\partial y} + \gamma \tilde{n} + D \frac{\partial^2 \tilde{n}}{\partial y^2} - DL \nabla \frac{\partial \tilde{n}}{\partial y} \times z \cdot \nabla \tilde{n}$$
$$+ \rho c_s \nabla \tilde{n} \times z \cdot \nabla \rho^2 \nabla^2 \tilde{n} + \mu \nabla^4 \tilde{n} = 0 , \quad (10)$$

where $\tilde{n}$ is the fluctuating ion density, v^* is the diamagnetic drift-wave velocity $(cT_e/eB)/L$, L is a density gradient scale length, γ is a long-wavelength collisional damping coefficient, ρ is the ion gyroradius evaluated at the electron temperature, and c_s is the ion sound speed. D is a negative diffusivity describing the destablization of DTEM modes with $D = \varepsilon^{3/2} v^{*2}(1 + \frac{3}{2}\eta)/\gamma_e$, where γ_e is the electron collisional damping coefficient, ε is the inverse aspect ratio, and $\eta = d \ln T/d \ln n$ is the electron temperature gradient parameter. Finally, μ is the coefficient of hyperviscosity introduced to model strong damping at short wavelength. The important nonlinear terms are the fifth, which is the $E \times B$ nonlinearity, and the sixth, which is the polarization-drift nonlinearity.

The code is purely spectral, meaning all computations are done in Fourier space. The system is initialized with a mode spectrum symmetric about the origin and allowed to evolve until transient behavior has vanished. The magnetic field is oriented along the z axis, and the density gradient is in the x direction. In the jargon of the code, a 13×13 case contains the modes 0 though ± 6 in both the kx and ky directions, denoted by (ky, kx). For the work presented here the system was driven with a linear term (the fourth term) at long wavelengths. The intermediate-wavelength range of no damping or driving is known as the inertial range. Nondriven/nondamped systems were examined and appear also to be chaotic; however, we will concentrate here on the more physical model. Several cases were examined, including 13×13, 21×21, and 29×29. We present her the results for the 21×21 case, which are representative. The data analyzed include the fluctuating energy from each of the modes in the inertial and damped regimes and the total fluctuating energy and enstrophy (mean-squared vorticity). Results presented below indicate low-dimensional chaos and simple determinism in most cases examined with a dimension dependent on the regime.

TABLE I. Lyapunov exponents and Kaplan-Yorke dimension for two of the quantities analyzed from DEBS code.

| System	$10^3 \tau$ (units of τ_r)	D_{KY}	Lyapunov exponents		
dB_p/dt	0.96	5.31	0.3738 ± 0.0123	0.1247 ± 0.0091	0.0129 ± 0.0099
			-0.0535 ± 0.0112	-0.2184 ± 0.0177	-0.7796 ± 0.0343
	0.88	5.85	0.3638 ± 0.0106	0.1341 ± 0.0084	0.0113 ± 0.0085
			-0.0535 ± 0.0095	-0.1520 ± 0.0108	-0.3555 ± 0.0146
			-0.9002 ± 0.0288		
E_{ave}	0.96	6.30	0.3569 ± 0.0111	0.1537 ± 0.0092	0.0262 ± 0.0083
			-0.0033 ± 0.0033	-0.0760 ± 0.0113	-0.2296 ± 0.0142
			-0.7577 ± 0.0265		
	0.80	6.82	0.3680 ± 0.0103	0.1951 ± 0.0086	0.0404 ± 0.0076
			-0.0091 ± 0.0082	-0.0840 ± 0.0094	-0.1988 ± 0.0109
			-0.3791 ± 0.0144	-0.9597 ± 0.0288	
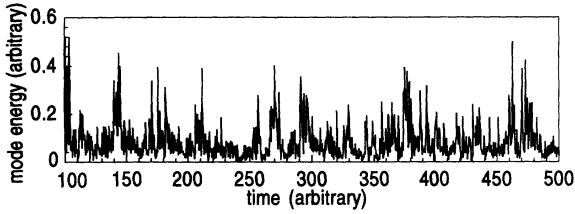
FIG. 4. Energy of the (0,8) mode of a 21×21 mode system in the DTEM model. This mode is in the damped regime.

Figure 4 shows a typical time trace of the (0,8) mode energy. This mode is part of the damped regime. Figure 5 shows the correlation dimension for the (0,6) mode, part of the inertial range, and its phase-randomized surrogate. There is a plateau region at a dimension near 6 that is not evident in the surrogate plot. The divot seen in the surrogate plot near a dimension of 7 is typical of the spurious plateau seen with correlated noise. Modes in the damped regime also indicate low-dimensional dynamics, with a dimension near 9. The measured dimension of the inertial range is typically lower than that of the damped regime; however, no strong dependence with mode number is seen for modes in the same regime. This behavior is not unreasonable and is consistent with the results reported in [7]: the regime in which the linear terms dominate (damping regime) shows a higher dimension than does the regime in which nonlinear terms dominate (inertial range).

Figure 6 demonstrates the short-term predictability of the signals. Plotted are the prediction errors from the (0,6) mode, the (0,8) mode and the total energy along with the error of their phase-randomized surrogates. The short-term predictability of the (0,8) mode is especially good: at least an order of magnitude better than its surrogate. The predictability of the energy is also good, though not quite as dramatic as the (0,8) mode. The predictability of the (0,6) mode is very poor, though, showing a large prediction error comparable with its surrogate's.

One should expect a system to have a single dimension characterizing its topological structure. We can offer some speculation as to why different modes show different dimensions and predictability. The DTEM
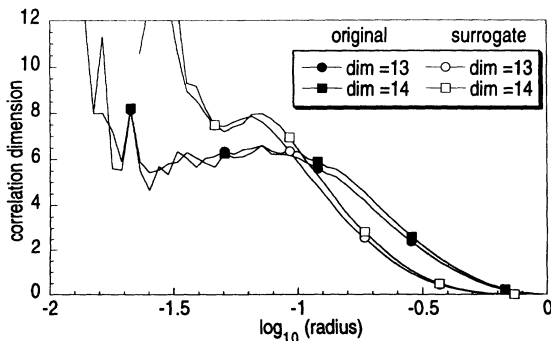

FIG. 5. Correlation dimension of the (0,6) mode of DTEM model. There is a clear scaling region for the original signal at a dimension between 8 and 9 not evident in the surrogate.
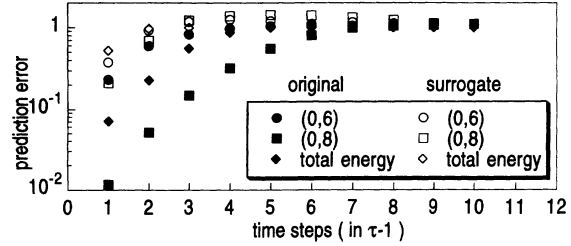

FIG. 6. Prediction error for the (0,6), (0,8) modes and total energy of the 21×21 mode spectrum. Predictability is good for both the (0,8) mode and the total energy, though poor for the (0,6) mode.

model has two very different regimes, the inertial range and damped regime, which govern the dynamics of the system. In the inertial range the only dissipation is through the nonlinear coupling to the other modes, while the damping regime contains a dominant linear damping term. The dynamics of the damping regime are largely independent of the inertial range; the reverse, however, is not true. Thus, it may not be unreasonable that the two regimes have different dimensions when examining the large-scale structure. At very small scales this difference should disappear, reflecting the fact that it is a coupled system. However, the number of points required and computational constraints restrict the ability to explore this limit of infinitesimal scale. Because the inertial range is very nearly Hamiltonian, trajectories are not strongly drawn to the attractor. Through the interaction with other modes, modes in this regime may experience perturbations from the inertial manifold of the attractor, and cannot quickly return to the manifold. In the damped regime, the dominant linear term ensures that the trajectory remains close to the inertial manifold, accounting for its superior predictability.

Table II shows the Lyapunov exponents for the (0,6) and (0,8) modes in several embedding dimensions. Both systems have positive exponents, indicating that the modes are chaotic. The (0,8) mode has a higher Kaplan-Yorke dimension before it saturates, as expected. The exponents are very stable from one embedding to the next, remaining at approximately the same value. This is a good indication that the values are probably very nearly correct. In addition, both show at least one and possibly two zero values.

IV. EXPERIMENTAL DATA FROM THE MADISON SYMMETRIC TORUS

To ascertain whether or not simple determinism governs discharges in the Madison Symmetric Torus a wide range of signals was analyzed comprising both global and local measurements. Global signals included fluctuations in the average toroidal magnetic field at the wall, dB_{tw}/dt, fluctuations in the plasma current, dI_p/dt, chord averaged density fluctuations, both optical and soft x-ray radiation, and toroidal and poloidal gap voltages V_{tg} and V_{pg}. Local signals included local poloidal and toroidal magnetic field fluctuations, ion saturation

TABLE II. Lyapunov exponents and Kaplan-Yorke dimension for two modes of the DTEM model. Time units are proportional to $1/v^*$.

System	τ	D_{KY}	Lyapunov exponents		
Mode (0,6)	0.18	8.10	1.7775 ± 0.0427	1.0174 ± 0.0315	0.5018 ± 0.0276
			0.0950 ± 0.0260	-0.0222 ± 0.0222	-0.4130 ± 0.0335
			-0.9218 ± 0.0396	-1.6575 ± 0.0564	-3.8867 ± 0.1088
	0.16	8.55	1.7148 ± 0.0377	0.9704 ± 0.0301	0.4574 ± 0.0261
			0.0757 ± 0.0235	-0.0525 ± 0.0268	-0.2167 ± 0.0290
			-0.6746 ± 0.0337	-1.1945 ± 0.0430	-1.9802 ± 0.0594
			-4.4591 ± 0.1159		
Mode (0,8)	0.05	9.09	8.8462 ± 0.1415	4.9430 ± 0.1087	2.5281 ± 0.0860
			1.1518 ± 0.0841	0.0490 ± 0.0490	-0.3610 ± 0.0996
			-1.2486 ± 0.1249	-3.9239 ± 0.2864	-9.2991 ± 0.5115
			-29.022 ± 1.073		
	0.04	9.63	8.9888 ± 0.1169	5.7238 ± 0.1030	3.3122 ± 0.0894
			1.3845 ± 0.0872	0.1431 ± 0.0976	-0.4498 ± 0.1183
			-1.9071 ± 0.1354	-3.7892 ± 0.1629	-6.5160 ± 0.1955
			-10.868 ± 0.250	-23.434 ± 0.0398	

current J_{sat}, and plasma potential fluctuations. We present here a representative sample drawn from both groups.

The data were taken during the 40-ms flattop period of the MST discharge, which is the period over which the system is most nearly stationary. The global magnetic fields of a typical low current discharge ($\sim$290 kA) are shown in Fig. 7. Most signals were digitized at either 250 or 500 kHz, resulting in 10 000 to 20 000 points. The power spectra of all signals are broadband, with significant power in most up to 100 kHz. The autocorrelation times are extremely short, on the order of two to three times steps for all signals except J_{sat}. dB_{tw}/dt is plotted in Fig. 8. Evident in all signals are the flux jumps, bursts of magnetic field energy, which are characteristic of the MST discharges.

Figure 9 shows a comparison of the correlation dimension of dB_{tw}/dt and its phase-randomized surrogate. There is no saturation to a plateau with increasing embedding for any signal, 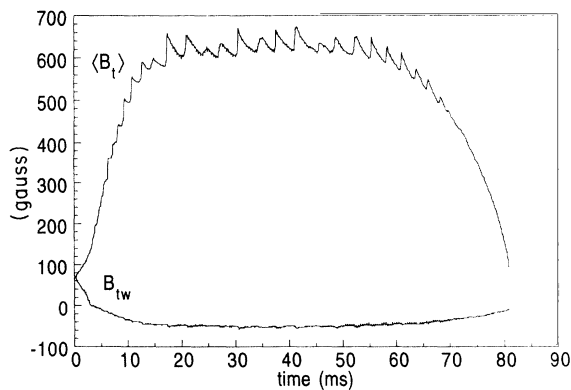indicating that there is no evidence for low-dimensional chaos or simple determinism in the unprocessed signals from MST. The curves of the original and surrogate data are indistinguishable, confirming that dB_{tw}/dt is not a low-dimensional chaotic process. Figure 10 depicts the prediction error for the MST signals. None of the signals are predictable in the short term. The steep rise from a modestly high value (20–30 %) to saturation at 100% within two to three time steps is typical of correlated noise.

Table III presents the calculated Lyapunov exponents for the data. With each increase in embedding, the Kaplan-Yorke (KY) dimension increases significantly, although it does not equal the embedding dimension. Several of the signals, J_{sat}, dB_t/dt, and dB_p/dt, do show credible zero exponents, which would indicate that the processes are continuous in time rather than random fluctuations. dB_{tw}/dt and dI_p/dt do not show a zero exponent. Because the KY dimension never saturates, the negative Lyapunov exponents cannot be trusted, despite the fact that some of the larger values appear relatively stationary. The positive values may be correct and reflect the space-filling property of the high-dimensional system.

In addition to time-series analysis, MST discharges were analyzed spatially using a set of magnetic pickup coils distributed toroidally around the torus. Rather than using time-delay embeddings to reconstruct the
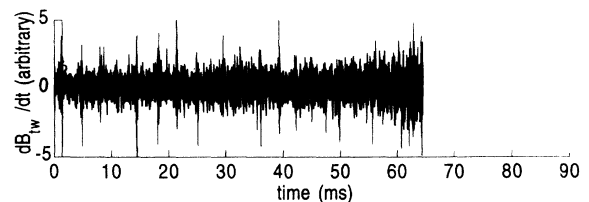

FIG. 7. Magnetic fields for a typical MST discharge. The data presented here were analyzed during the flattop period about 17–57 ms.

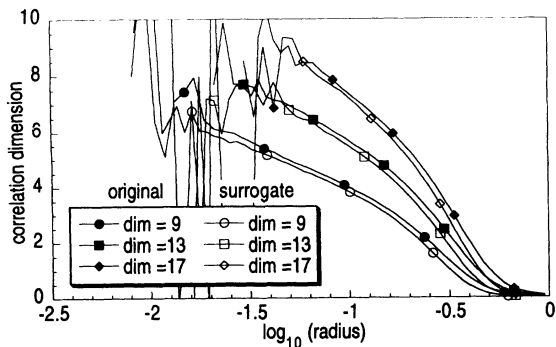FIG. 8. Fluctuations in the toroidal magnetic field at the wall in the MST.

FIG. 9. Comparison of the correlation dimension of dB_{tw}/dt in MST with its surrogate data set. Both show very similar behavior, indicating that dB_{tw}/dt is not governed by a low-dimensional chaotic process.
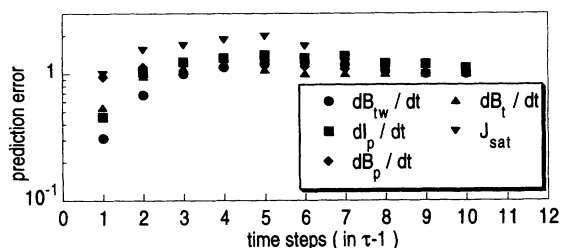

FIG. 10. Prediction error for MST signals. None show any short-term predictability beyond that of correlated noise.

phase space, vectors were created by using signals from separate coils as individual vector components. The purpose was to address the issue of stationarity by analyzing data from a very short time period and still have a sufficient number of vectors for adequate analysis. The correlation integral was computed using 2000 of these "spatial" vectors over a duration of 4 ms of the discharge in embeddings up to 9. The number of coils corresponds to the embedding dimension. The results are consistent with the time series analysis. No evidence for simple determinism was seen in MST discharges.

Although there is no evidence for simple determinism in the raw data, the possibility remains that the signals are noise corrupted. Nonlinear noise reduction was applied to all signals in an attempt to extract an underlying low-dimensional system. Figure 11 shows the effect of the filter on dB_{tw}/dt after six iterations. Qualitatively, the two signals do not differ significantly from one another. The nonlinear-noise-reduction method is most effective if the time scale of the noise is significantly shorter than the time scale of the underlying dynamical system. These results indicate that this is not the case for MST signals.

The correlation dimension for dB_{tw}/dt after noise reduction is plotted in Fig. 12. There is still no evidence of low-dimensional chaos in this or any of the data. Figure 13 shows the prediction error for the MST signals after nonlinear noise reduction. They actually show poorer predictive behavior than before filtering.

TABLE III. Lyapunov exponents for the MST signals, measured in μs^{-1}, and corresponding Kaplan-Yorke dimensions.

| Signal	τ (μs)	D_{KY}	Lyapunov exponents		
dB_{tw}/dt	2	4.02	0.1570 ± 0.0011	0.0691 ± 0.0012	-0.0342 ± 0.0018
			-0.1790 ± 0.0029	-0.5480 ± 0.0049	
		6.15	0.1186 ± 0.0008	0.0701 ± 0.0008	0.0288 ± 0.0009
			-0.0162 ± 0.0012	-0.0569 ± 0.0017	-0.1134 ± 0.0028
			-0.2057 ± 0.0029	-0.4776 ± 0.0043	
dI_p/dt	2	4.11	0.1589 ± 0.0011	0.0670 ± 0.0012	-0.0205 ± 0.0016
			-0.1472 ± 0.0026	-0.5068 ± 0.0046	
		6.24	0.1227 ± 0.0009	0.0726 ± 0.0008	0.0296 ± 0.0009
			0.0093 ± 0.0011	-0.0536 ± 0.0016	-0.1100 ± 0.0023
			-0.2157 ± 0.0030	-0.4987 ± 0.0045	
J_{sat}	10	4.09	0.0432 ± 0.0021	0.0159 ± 0.0021	-0.0081 ± 0.0024
			-0.0411 ± 0.0032	-0.1047 ± 0.0059	
		5.07	0.0509 ± 0.0023	0.0232 ± 0.0018	0.0019 ± 0.0019
			-0.0181 ± 0.0024	-0.0481 ± 0.0035	-0.1427 ± 0.0073
dB_p/dt	4	4.04	0.0670 ± 0.0009	0.0257 ± 0.0009	-0.0149 ± 0.0011
			-0.0636 ± 0.0015	-0.1731 ± 0.0028	
		6.66	0.0567 ± 0.0009	0.0342 ± 0.0007	0.0147 ± 0.0006
			-0.0009 ± 0.0007	-0.0174 ± 0.0008	-0.0399 ± 0.0010
			-0.0723 ± 0.0014	-0.1751 ± 0.0028	
dB_t/dt	4	4.19	0.0698 ± 0.0010	0.0317 ± 0.0009	-0.0102 ± 0.0011
			-0.0599 ± 0.0016	-0.1645 ± 0.0028	
		6.77	0.0581 ± 0.0009	0.0350 ± 0.0007	0.0169 ± 0.0006
			0.0005 ± 0.0005	-0.0173 ± 0.0008	-0.0377 ± 0.0009
			-0.0718 ± 0.0014	-0.1708 ± 0.0027	
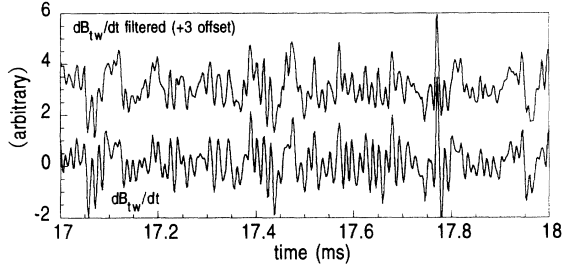
FIG. 11. Effect of nonlinear noise reduction on dB_{tw}/dt. The original and noise reduced signal are nearly identical.

FIG. 13. Prediction error for MST signals after processing with the nonlinear filter. Predictability has deteriorated in most signals relative to the unfiltered case (cf. Fig. 10).

V. CONCLUSIONS

A. Summary

In this paper we examine the possibility that low-dimensional chaos and simple determinism govern the dynamics of RFP plasma discharges using both experimental and numerical simulation data. In addition, several quantities have been measured to characterize fully the nonlinear dynamics.

Data from both numerical simulations show strong evidence for low-dimensional chaos. The DEBS code, which models RFP discharges, shows a correlation dimension between 3 and 4 in both magnetic and electric field fluctuations. The spectrum of Lyapunov exponents gives a correspondingly low value for the Kaplan-Yorke dimension. Most signals indicate simple determinism with good short-term predictability. Mode energies of the DTEM model, which simulates long-wavelength drift-wave turbulence, also have a low correlation dimension, with a value near 6 for modes in the damped regime and near 9 for modes in the inertial range. Predictability is good for all cases, though better for modes in the damped regime than for those in the inertial range. The measured Lyapunov exponents corroborate these findings.

Many local and global signals from the Madison Symmetric Torus were analyzed. Despite concerted effort, including the application of linear and nonlinear filtering techniques, no evidence of low-dimensional chaos or simple determinism is found. There is no clear scaling region
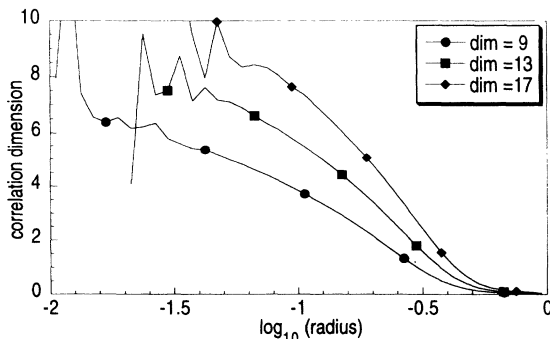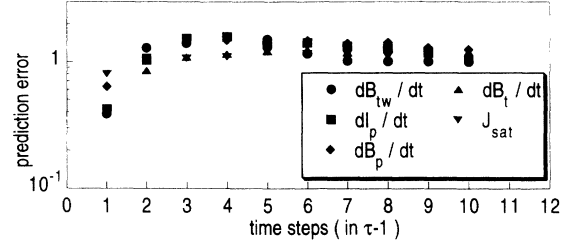

FIG. 12. Correlation dimension of dB_{tw}/dt from the MST signals after processing with the nonlinear-noise-reduction method. There are still no indications of low-dimensional chaos.

for the correlation integral, nor does the Kaplan-Yorke dimension saturate. All data have poor short-term predictability.

B. Discussion

The fact that the experimental data from the MST show no simple determinism must be contrasted with the positive results of both the numerical simulations and previous results from other experiments. The discrepancy between code and experiment has several likely origins. The DEBS code, although it seems to model some RFP processes well, contains several crucial simplifications. The model lacks temperature and pressure effects. Another simplification is the small number of modes. The 27 modes (9 toroidal by 3 poloidal) used in the DEBS code are probability far too few to model the highly turbulent system of the experiment. The different Lundquist numbers also probably contributes to the difference between the experiment and simulation since the nonlinear interaction among the modes increases with Lundquist number. Finally, in order to efficiently model the long-wavelength tearing modes of the plasma, the code does not treat fast fluctuations correctly. The broadband nature of the experimental data indicates that these high-frequency oscillations may be important to the system dynamics. One could reasonably expect that the dimension should increase significantly if some or all of these simplifications were rectified in the model.

That low-dimensional chaos is seen in the DTEM model and not in the experimental data from MST may not be too disconcerting since drift-wave turbulence is believed not to be significant in RFP plasmas. Yet the model is in many ways general enough that one might expect to see similar results despite this difference. The code suggests that one should see simple determinism in individual mode amplitudes. However, analysis of individual mode amplitudes from magnetic fluctuations in MST yielded negative results. The simulation models only one of several processes occurring simultaneously in a real plasma. This omission could account for the difference.

There may be several obstacles that hinder the identification of low-dimensional dynamics in the experiment. Apparent from the signals is that the magnetic flux jumps are a dominant feature. Yet the data records, due to the discharge length, contain only a few flux jumps. Typically, one requires several hundred cycle times of the "dominant" period of the system for proper

estimation of the dimension. A related problem is that, if the system is high dimensional, many more points are needed to estimate that dimension.

A second, and probably more important, concern is the issue of stationarity. Even a very small random fluctuation in one of the system parameters can make the dimension immeasurable. One possible such process is the influx of impurity ions into the plasma. Nonrandom (deterministic) perturbations can increase the dimension by at most 1 for each fluctuating quantity. However, if several presumably stationary parameters (e.g., loop voltage or primary current) fluctuate this may put impractical limits on the number of points required to estimate the dimension.

On the basis of our analysis we must conclude that the dynamics of the RFP is probably high dimensional. When analyzing a system, even if all parameters— embedding delay time, embedding dimension, number of points, etc.—are not optimally determined there is at least some indication of a plateau in the correlation dimension plots. The data from the MST show not the slightest hint of a plateau, even for embeddings up to 30. The behavior of the correlation plots is very similar to high dimensional or random data. We estimate that the dimension is probably greater than 15, using the criterion in [19] with 20 000 points and a minimum plateau length of 0.2 decades in r. Our results make us skeptical of previously reported claims of low dimensionality in turbulent magnetoplasmas.

ACKNOWLEDGMENTS

[1] C. W. Horton and L. Reichel, *Statistical Physics and Chaos in Fusion Plasmas* (New York, 1984).

[2] T. Braun, J. Lisboa, and J. Gallas, Phys. Rev. Lett. **68**, 2770 (1992).

[3] J. Qin, L. Wang, D. Yuan, P. Gao, and B. Zhang, Phys. Rev. Lett. **63**, 163 (1989).

[4] P. Cheung and A. Wong, Phys. Rev. Lett. **59** (1987).

[5] J. H. Chu and L. I, Phys. Rev. A **39**, 233 (1989).

[6] G. Strohlein and A. Piel, Phys. Fluids B **1**, 1168 (1989).

[7] M. Persson and H. Nordman, Phys. Rev. Lett. **67**, 3396 (1991).

[8] W. Arter and D. N. Edwards, Phys. Lett. **114A**, 84 (1986).

[9] S. J. Gee and J. B. Taylor (unpublished).

[10] H. J. Barkley, J. Andreoletti, F. Gervais, J. Olivain, A. Quemeneur, and A. Truc, Plasma Phys. **30**, 217 (1988).

[11] M. L. Sawley, W. Simm, and A. Pochelon, Phys. Fluids **30**, 129 (1987).

[12] R. N. Dexter, D. W. Kerst, T. W. Lovell, S. C. Prager, and J. C. Sprott, Fusion Technol. **19**, 131 (1991).

[13] S. Assadi, Phys. Rev. Lett. **69**, 281 (1992).

[14] F. Takens, in *Dynamical Systems of Turbulence*, edited by D. A. Rand and L. S. Young, Lecture Notes in Mathematics Vol. 898 (Springer, Berlin, 1981), p. 366.

[15] A. M. Albano, J. Muench, and C. Schwartz, Phys. Rev. A **38**, 3017 (1988).

[16] P. Grassberger and I. Procaccia, Phys. Rev. Lett. **50**, 346 (1983).

[17] J. W. Havstad and C. Ehlers, Phys. Rev. A **39**, 845 (1989).

[18] L. Smith, Phys. Lett. A **133**, 283 (1988).

[19] A. Tsonis, *Chaos: From Theory to Applications* (Plenum, New York, 1992).

[20] D. Ruelle, Proc. R. Soc. London, Ser. A **427**, 241 (1990).

[21] J. P. Eckmann and D. Ruelle, Rev. Mod. Phys. **57**, 617 (1985).

[22] A. Wolf, J. Swift, H. Swinney, and J. Vastano, Physica D **16**, 285 (1985).

[23] H. Haken, Phys. Lett. **94A**, 71 (1983).

[24] J. P. Eckmann, S. O. Kamphorst, D. Ruelle, and S. Ciliberto, Phys. Rev. A **34**, 4971 (1986).

[25] K. Briggs, Phys. Lett. A **151**, 27 (1990).

[26] J. H. Wilkinson and C. Reinsch, *Linear Algebra* (Springer, Berlin, 1971).

[27] LAPACK FORTRAN *Routines*, available by anonymous ftp from netlib@research.att.com

[28] J. Kaplan and J. Yorke, in *Chaotic Behavior of Multidimensional Difference Equations*, edited by H. Peitgen and H. W. W. (Springer, New York, 1979).

[29] J. D. Farmer and J. Sidorwich, Phys. Rev. Lett. **59**, 845 (1987).

[30] G. Sugihara and R. May, Nature **344**, 734 (1990).

[31] R. Wayland, D. Bromley, D. Pickett, and A. Passamante, Phys. Rev. Lett. **70**, 580 (1993).

[32] E. J. Kostelich and J. A. Yorke, Phys. Rev. A **38**, 1649 (1988).

[33] T. Schreiber and P. Grassberger, Phys. Lett. A **160**, 411 (1991).

[34] T. Sauer, Physica D **58**, 193 (1992).

[35] R. Cawley and G. H. Hsu, Phys. Rev. A **46**, 3057 (1992).

[36] P. Grassberger, T. Hegger, H. Kantz, C. Schaffrath, and T. Schreiber, Chaos **3**, 127 (1993).

[37] N. Enge, T. Buzug, and G. Pfister, Phys. Lett. A **175**, 178 (1993).

[38] T. Schreiber, Phys. Rev. E **47**, 2401 (1993).

[39] D. S. Harned and D. D. Schnack, J. Comput. Phys. **65**, 57 (1986).

[40] P. Kirby, Comput. Phys. **47**, 17 (1987).

[41] D. D. Schnack, D. C. Barnes, Z. Mikic, D. S. Harned, and E. J. Caramana, J. Comput. Phys. **70**, 330 (1987).

[42] Y. L. Ho, Ph.D. thesis, University of Wisconsin—Madison, 1989 (unpublished).

[43] R. J. Fonck, S. F. Paul, D. R. Roberts, Y. J. Kim, N. Bretz, D. Johnson, R. Nazikian, and G. Taylor (unpublished).

[44] P. Cripwell and A. E. Costley (unpublished).

[45] D. L. Brower, W. A. Peebles, and N. C. Luhmann, Nucl. Fusion **27**, 2055 (1987).

[46] P. W. Terry and W. Horton, Phys. Fluids **25**, 491 (1982).

[47] D. E. Newman, P. W. Terry, P. H. Diamond, and Y.-M. Liang, Phys. Fluids B **5**, 1140 (1993).